# Tough-brittle transition in the planar fracture of unidirectional fibre composites

Uttam S Kachhwah and Sivasambu Mahesh*

*Department of Aerospace Engineering,*

*Indian Institute of Technology Madras, Chennai 600 036, India.*

## Abstract

The transverse fracture of model unidirectional composite specimen, comprising up to $2^{20}$ fibres with random strengths, is studied using Monte Carlo simulations. The load-sharing from broken to intact fibres is assumed to obey power-law scaling $\sim r^{-\gamma}$ with distance $r$ from the fibre break. Fibre breaks are assumed to interact in order to remain traction free. The pattern of fibre breaks that propagate catastrophically is interpreted through cluster analysis. The empirical strength distributions obtained from the simulations are interpreted using two probabilistic models of brittle fracture available in the literature. These point to a transition from the brittle to the tough fracture mode as $\gamma \downarrow 2$. The transitional $\gamma$ is approximately equal to that reported in the literature for non-interacting fibre breaks.



**PACS numbers:** 72.80.Tm, 02.50.Ey, 02.70.ac, 05.10.Ln


## I. INTRODUCTION

Unidirectional fibre composites loaded in uniaxial tension along the fibre direction are model heterogeneous materials. In general, the fracture of these materials, entails the formation of fibre breaks, matrix cracks, and interfacial debonds in three dimensions [1, 2]. However, in polymer matrix unidirectional composites with a well-bonded fibre-matrix interface, it is reasonable to treat the fracture process as being localised in a plane transverse to the fibre direction by (i) regarding the composite as a chain of independent longitudinal segments [3, 4], the failure of one of which amounts to composite failure, and (ii) by conservatively assuming that fibre breaks in each segment occur in a common transverse plane [5, 6]. The assumption of fracture processes being confined to a transverse plane has often been used in the literature [6–10] to study the modes of development of fracture, and to obtain the strength distributions of heterogeneous materials. This assumption is adopted in the present study also.

It is clear from the foregoing studies that the fracture mode depends on the variability of fibre strengths. The fibre length relevant to the present two-dimensional setting is one segment long. Taking this length to be unity, and assuming the normalised fibre strengths


* smahesh@iitm.ac.in

to be Weibull [11] distributed, the distribution function for the random fibre strength, $\Sigma$, is given by:

$$F(\sigma) = \Pr\{\Sigma < \sigma\} = 1 - \exp(-\sigma^{\rho}), \tag{1}$$

where $\rho > 0$ is termed the Weibull modulus.

Besides the fibre strength variability, fracture development and strength distribution of two-dimensional unidirectional composite bundles also depends sensitively on the load redistribution amongst the surviving fibres due to fibre failure [7, 8, 10, 12], i.e., the load sharing rule. Equal load sharing (ELS), and local load sharing (LLS) are limiting load sharing rules. In ELS, the load dropped by a broken fibre is distributed equally among all the surviving fibres. In ELS composites subjected to monotonically increasing tensile load, the locations of fibre breaks are uncorrelated, and the fracture mode is tough. ELS composite strength obeys a Gaussian distribution [13]. In LLS, the load dropped by the broken fibres is distributed entirely amongst their nearest intact neighbours. Under LLS, fibre break positions are highly correlated, and the composite suffers brittle fracture, regardless of the scatter in the random tensile strengths of the fibres. That is, fracture proceeds by the catastrophic growth of a localised cluster of breaks. Composite strength obeys weakest-link scaling, and a probabilistic model for the weakest-link event is known [9, 14, 15].

It is clear from the above that the fracture mode transitions from tough to brittle when the load sharing changes from ELS to LLS. The precise location of the transition, for various interpolation schemes between ELS and LLS, has been studied in the literature. Hidalgo *et al.* [7] considered a square patch with periodic boundary conditions. In a patch with only one broken fibre, they assumed that the stress concentration, $K(r)$, in a surviving fibre distant $r$ from the broken fibre obeys the power law

$$K(r) = 1 + c\, r^{-\gamma}, \tag{2}$$

where $\gamma \geq 0$. Parameter $c$ is obtained by demanding that the stress overloads (i.e., stress concentrations less unity) add up to unity, i.e.,

$$\sum_{r>0}(K(r) - 1) = 1, \text{ i.e., } c = \left[\sum_{r>0} r^{-\gamma}\right]^{-1}. \tag{3}$$

It is clear that $c = c(\gamma, N)$ depends on the load sharing exponent, and the system size. The overload profile in Eq. (2) coincides with ELS for $\gamma = 0$, and with LLS for $\gamma \to \infty$. Hidalgo

*et al.* [7] and Roy *et al.* [10] found that brittle fracture is obtained for $\gamma \gtrsim 2.17$, while tough characteristics are obtained for smaller $\gamma$.

In an infinite patch, the summation of Eq. (3) can be approximated as:

$$c = \left[\sum_{r=1}^{\infty} \frac{1}{r^{\gamma}}(2\pi r)\right]^{-1} \sim \left[\sum_{r=1}^{\infty} \frac{1}{r^{\gamma-1}}\right]^{-1}. \tag{4}$$

The latter sum converges for $\gamma > 2$, so that $c$ is independent of $N$, for sufficiently large $N$. For $\gamma \leq 2$, however, the sum in the right side of Eq. (4) diverges. This means that in a finite simulation cell with $N$ fibres, $c \downarrow 0$ with increasing $N$. The overload profile due to a single break thus depends not only on the power-law exponent, $\gamma$, but also on the simulation cell size, $N$, even for large $N$, if $\gamma \leq 2$.

Another interpolation scheme between the ELS and LLS limits is due to Pradhan *et al.* [8]. In their mixed-mode load sharing scheme, a fraction $g \in [0, 1]$ of the load dropped by the broken fibre is distributed equally amongst its nearest neighbours. The remainder, $1-g$, is distributed equally amongst all the surviving fibres. Clearly, the limits $g = 0$, and $g = 1$ correspond to the ELS and LLS limits. Pradhan *et al.* [8] showed that the tough-brittle transition for their model occurred at $g \approx 0.79$.

Roy *et al.* [10] have also proposed an interpolation scheme between ELS and LLS in two-dimensions. In their scheme, the load of the broken fibre is distributed to surviving fibres in a rectangular region including the fibre, up to a specified distance $R$. This scheme too approximately interpolates between ELS and LLS as $R$ decreases from $\infty$ to 1. Roy *et al.* [10] found that the phase space spanned by fibre strength variability, and $R$ was sub-divided into six regions, which they termed brittle nucleating, brittle percolating, quasi-brittle nucleating, quasi-brittle percolating, high disorder limit, and temporally uncorrelated. Each phase describes a separate mode of fracture development.

Hidalgo *et al.* [7] and Roy *et al.* [10] assumed that the stress overload induced by a set of broken fibres at an intact fibre is simply the sum of the stress overloads due to the individual breaks. This assumption produces non-zero tractions at the fibre breaks, when more than one fibre is broken in the simulation cell. In physical composites, however, breaks interact to ensure zero traction at the fibre breaks. The opening displacement of each break is altered by the presence of the other breaks, which is accounted for in the Hedgepeth model [16, 17]. Accounting for the interaction between breaks is also essential to capture the inverse square root decay of the stress fields with distance from the crack tip, comprised of a large number

of fibre breaks, in agreement with linear elastic fracture mechanics [5].

In the model of Pradhan *et al.* [8] too, fibre breaks do not interact. In this scheme, although zero traction is realised at fibre breaks, the stress state ahead of a large cluster of breaks does not follow the inverse square root decay with distance from the crack tip. Also, two fibre breaks that do not have a common neighbouring intact fibre, produce equal overload on their neighbours, regardless of the distance between the breaks, which is different from the response of an interacting elastic system [16–19].

On the one hand, the assumption of non-interaction between fibre breaks in the models of Hidalgo *et al.* [7], Pradhan *et al.* [8], and Roy *et al.* [10] makes the fracture simulations computationally light, and enables these studies to access large system sizes. On the other hand, the load sharing rules in these works is not representative of physically important elastic systems, such as fibre composites. Studies of the fracture modes in elastic systems, on the other hand, have been limited to small system sizes of the order of a few thousand fibres, to keep the computational effort tractable [6, 20]. While these studies are able to identify the brittle fracture mode as such, it is not clear if the tough modes observed represent size-independent response, or are an artefact of limited system size [6].

In recent work, an algorithm based on the fast Fourier transform has been developed to simulate fracture of a two dimensional transverse plane [21, 22]. These simulations are asymptotically faster than the classical simulations, and can access composite bundles comprised of millions of fibres, while accounting for elastic interactions between fibre breaks. Also, although Gupta *et al.* [21], and Mahesh *et al.* [22] assumed Hedgepeth load sharing, the methodology developed therein can be applied to arbitrary load sharing rules, including Eq. (2). These advantages mitigate the simulation cell size limitations of fracture simulations in elastic composites [6, 19], and open up the possibility of exploring the tough-brittle transition through fracture simulations.

As in Hidalgo *et al.* [7], Pradhan *et al.* [8], and Roy *et al.* [10], it is attempted in the present work to identify the $\gamma^*$ at which the tough-brittle transition occurs in the transverse fracture of unidirectional composites. The difference between those works, and the present one is that the elastic interactions among fibre breaks is accounted for, so that fibre breaks in the present work are traction free. The stress concentration at the edge of a cluster of interacting fibre breaks is greater than the simple sum of the stress concentrations induced by non-interacting fibre breaks [6, 17, 19]. The increased stress concentration may promote

the brittle fracture mode, and may thereby decrease the value of $\gamma^*$.

In Sec. II, the simulation methodology, cluster analysis tools, and probabilistic models are recollected. Empirical strength distributions obtained from the simulations are presented in Sec. III, and interpreted using the probabilistic model based on tight cluster growth [9]. The use of probabilistic fracture models to identify the tough-brittle transition is a novel feature of the present work. Of central importance in this analysis is the size of the critical cluster of fibre breaks, which triggers catastrophic crack growth. It is shown that the size of the critical cluster scales as the system size for $\gamma \approx 2$, but scales slower than the system size for $\gamma > 2$. This points to a tough-brittle transition very near $\gamma = 2$, even when fibre breaks interactions are accounted for.

## II. FRACTURE MODES

### II.1. Computational

#### *II.1.1. Fracture simulations*

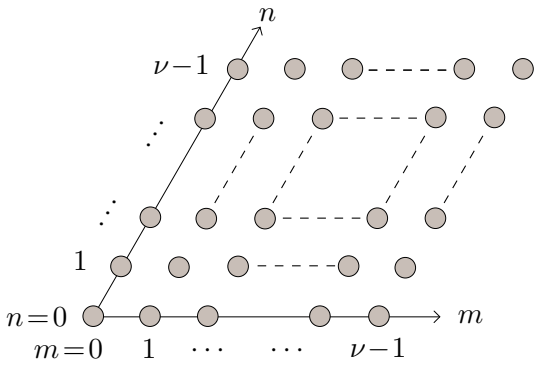


FIG. 1: A rhombus-shaped periodic simulation cell of $\nu \times \nu$ fibers arranged in a hexagonal lattice showing the $m$–$n$ coordinate system.

Monte Carlo simulations are performed in rhombus-shaped patches representing a transverse cross-section of the fibre composite. The transverse cross-section is comprised of $N = \nu \times \nu$ fibres, as shown in Fig. 1. $N$ is termed the system size. The $m$-$n$ coordinate system to locate fibres in the simulation cell is also shown. Periodic conditions are imposed so that the row of fibres at the left and right edges ($m = 0$ and $m = \nu - 1$) are

neighbours. Similarly, the fibres at the bottom and top edges ($n = 0$ and $n = \nu - 1$) are also considered neighbours. The periodic boundary conditions ensure that the stress concentrations induced by a single break is translation invariant, i.e., only the separation between the broken fibre and a surviving fibre is important for determining the stress concentration in the latter, due to the former, and not the absolute positions of the two fibres. This property makes the matrix $[\Lambda]$, whose element $\Lambda_{mnpq}$ represents the stress overload in fibre $(p, q)$ due to a fibre break at $(m, n)$, circulant in two modes [23]. The circulance of $[\Lambda]$ enables it to be diagonalised asymptotically faster in Fourier space than in real space, as detailed in Gupta *et al.* [21], and enables an asymptotically faster solution for the opening displacements at the fibre breaks.

The computational time of the Monte Carlo simulations can also be decreased by a considerable factor by noticing that in a two-dimensional simulation cell, the stress overload in a surviving fibre increases monotonically with the number of fibre breaks. This enables the determination of the ultimate tensile strength of the simulation cell to any desired accuracy using successive bisection. If the ultimate tensile strength of the composite can be bracketed tightly, this proves to be much faster than the commonly followed approach [6, 24] of gradually increasing the applied load up to the point of catastrophic crack growth, as detailed in Mahesh *et al.* [22].

For each Weibull exponent $\rho$, and system size, $N$, $N_{\mathrm{sim}}$ statistically identical composite specimen are generated by assigning fibre strengths drawn from Eq. (1). Let $\bar{\sigma}_{(i)}$ denote the strength of the $i$-th weakest specimen, for $i \in \{1, 2, \ldots, N_{\mathrm{sim}}\}$. The empirical strength distribution, $G_N(\sigma_{(i)}; \gamma, \rho)$ is then defined as

$$G_N(\sigma_{(i)}; \gamma, \rho) = \frac{i - 1/2}{N_{\mathrm{sim}}}, \tag{5}$$

for $i \in \{1, 2, \ldots, N_{\mathrm{sim}}\}$.

### *II.1.2. Cluster analysis*

The fracture mode – tough, or brittle – can sometimes be identified visually by examining snapshots of fracture development [6]. Clustering together of breaks into a critical cluster, and their propagation suggests brittle fracture. However, seemingly disperse fibre breakage can also cause brittle fracture [22]. Visual identification of the fracture mode may thus be

erroneous.

Kun *et al.* [25], Hidalgo *et al.* [7], Pradhan *et al.* [8], Roy *et al.* [10], and others have used a quantitative method to identify the fracture mode, based on cluster analysis. In this method, the frequency $f(s)$ of clusters of fibre breaks of size $s$ is obtained just before catastrophic crack growth begins. The moments of $f(s)$, defined as:

$$M_k = \sum_s s^k f(s), \tag{6}$$

are calculated for $k \in \{0, 1, 2, \ldots\}$. $M_0$ and $M_1$ represent the number of clusters, and the number of broken fibres, respectively. Hidalgo *et al.* [7] have identified the $\gamma$ at which $M_2/M_1$ achieves a maximum with the brittle-ductile mode transition.

In the present setting, cluster analysis has been implemented using the classical Hoshen and Kopelman [26], and union-find [27, Sec. 22.3] algorithms. As noted in Sec. II.1.1, composite strength is determined presently by a bracketing procedure. The lower end point of the bracket signifies a load level at which the model composite survives. Cluster frequencies, $f(s)$, are calculated or recalculated at the lower end point whenever it is set, or updated. The $f(s)$ when the simulation terminates characterise the computational critical cluster, which propagates to rupture the remaining fibres. The moments, $M_k$ are calculated from $f(s)$, and the values of $M_k$ are averaged across the Monte Carlo simulations.

### II.2. Probabilistic models

The empirical strength distributions obtained from the Monte Carlo simulations will be interpreted using the probabilistic models of composite fracture, recalled below.

#### *II.2.1. Tough mode*

The prototypical example of a unidirectional tough composite is the loose bundle of threads studied by Daniels [13]. The load dropped by a broken fibre is redistributed equally amongst all the surviving fibres in a loose bundle of threads, following ELS. Qualitatively, in a tough composite, fracture occurs by the linking up of multiple clusters of fibre breaks spatially distributed over the entire cross-section. The number of fibre breaks in these clusters is comparable to the total number of fibres in the composite.

Consider a loose bundle of $M$ threads, whose strengths are Weibull [11] distributed, following Eq. (1). Then, the classical result of Daniels [13] states that as $M \to \infty$, the bundle strength per fibre, $E_M(\sigma)$, is Gaussian distributed:

$$E_M(\sigma) = \Phi\left(\frac{\sigma - \mu_M}{\sigma_M}\right) = \frac{1}{\sqrt{2\pi\sigma_M^2}} \exp\left(-\frac{(\sigma - \mu_M)^2}{2\sigma_M^2}\right), \tag{7}$$

with mean bundle strength [24],

$$\mu_M = (1/\rho)^{(1/\rho)} \exp(-1/\rho), \tag{8}$$

and standard deviation,

$$\sigma_M = \sqrt{\exp(-1/\rho)(1 - \exp(-1/\rho))/n}. \tag{9}$$

Eq. (7) is a good approximation of the bundle strength for large $M$. For smaller $M$, McCartney and Smith [28] have proposed a recursive formula for the strength of the $M$-bundle.

$$E_M(\sigma) = \{F(\sigma'_{M-1})\}^M - \sum_{k=0}^{M-1} \binom{M}{k} \Pi^{(k)} \{F(\sigma'_{M-1}) - F(\sigma'_k)\}^{M-k}. \tag{10}$$

In Eq. (10), $F(\cdot)$ is given by Eq. (1),

$$\Pi^{(k)} = \{F(\sigma'_{k-1})\}^m - \sum_{l=0}^{k-1} \binom{k}{l} \Pi^{(l)} \{F(\sigma'_{k-1}) - F(\sigma'_l)\}^{k-l},$$

$\binom{k}{l} = k!/(k!(k-l)!)$, $\sigma'_k = M\sigma/(M-k)$, and $\Pi^{(0)} = 1$. This formula becomes too computationally intensive, and prone to floating point truncation errors to use beyond about $M = 100$. Presently, therefore, the strength distribution is taken to follow Eq. (7) for $M > 100$, and to follow Eq. (10) for $1 \leq M \leq 100$.

The ELS bundle has been investigated extensively in the literature. Much is known about the fracture characteristics of ELS bundles, including the scaling of avalanche sizes, and energy released. These results may be found in Hansen *et al.* [29, Chap. 2, and 3].

### *II.2.2. Brittle mode*

The fracture of the composite bundle exhibits a brittle character when a localised cluster of fibre breaks forms, and propagates catastrophically. The number of fibre breaks in the localised cluster is much smaller than that in the composite. Let $G_N(\sigma; \gamma, \rho)$ denote the

empirical strength distribution, obtained from the Monte Carlo simulations, and defined in Eq. (5). Following Harlow and Phoenix [14], an unequivocal signature of the brittle mode is that the weakest-link empirical strength distribution,

$$W_N(\sigma;\gamma,\rho) = 1 - (1 - G_N(\sigma;\gamma,\rho))^{1/N}, \tag{11}$$

is independent of the number of fibres, $N$. Pictorially, the existence of a weakest-link failure event is confirmed by the collapse of plots of $W_N(\sigma;\gamma,\rho)$ for different system sizes $N$ into a common master curve. If $W_N$ were independent of $N$, it is reasonable to write $W(\sigma;\gamma,\rho)$, which now denotes the system-size independent strength distribution of the weakest-link failure event.

Two models available in the literature for predicting $W_N(\sigma;\gamma,\rho)$, viz., the Curtin [20] model, and the tight cluster growth model [9, 22, 30], are now summarised.

Curtin [20] proposed that composite failure occurs when at least one of $N/N_c$, $1 \leq N_c \leq N$ events occurs, the event being the failure of an $N_c$-bundle of fibres obeying ELS. Accordingly, the composite strength distribution, $G_N(\sigma;\gamma,\rho)$, is related to the strength distribution of the weakest-link event given by Eq. (7) through:

$$G_N(\sigma;\gamma,\rho) = 1 - \left(1 - E_{N_c}(\sigma;\mu'_{N_c})\right)^{N/N_c}. \tag{12}$$

Here, $E_{N_c}(\sigma;\mu'_{N_c})$ denotes the strength distribution of an $N_c$ fibre ELS bundle, with $M = N_c$, and standard deviation given by Eq. (9). The mean, $\mu'_{N_c}$, of $E_{N_c}(\sigma;\mu'_{N_c})$ generally differs from that given by Eq. (8). The shifted mean, $\mu'_{N_c}$, and the size of the weakest-link, $N_c$ are the two parameters of the Curtin [20] model.

It follows from Eqs. (11), and (12) that

$$W_N(\sigma;\gamma,\rho) = 1 - (1 - E_{N_c}(\sigma))^{1/N_c}. \tag{13}$$

The Curtin [20] model regards the $N_c$-cluster of fibre breaks as the nucleus of brittle fracture; fibres ahead of this cluster are assumed to break almost surely, i.e., with probability 1.

The following procedure is used to fit the parameters of the Curtin [20] model. For each $N'_c \in \{1, 2, \ldots, N\}$, the empirical distribution, $1 - (1 - G_N(\sigma_{(i)};\gamma,\rho))^{N'_c/N}$, is plotted on Gaussian probability coordinates. The empirical distribution is assumed Gaussian distributed, and a minimum least-squares straight line is fit to it. The reciprocal of the slope of this straight line gives the standard deviation of the empirical distribution. The empirical

standard deviation so obtained is compared with the standard deviation of the Daniels distribution, Eq. (9), with $M = N_c'$. The $N_c'$ for which the relative error between the empirical and Daniels standard deviations is the least is considered the best fit. The corresponding $N_c'$ is taken to be $N_c$. With $N_c$ fit, $\mu'_{N_c}$ is fixed by determining the translation to be applied to the mean of the model predicted strength distribution so that it matches the mean of the empirical strength distribution.

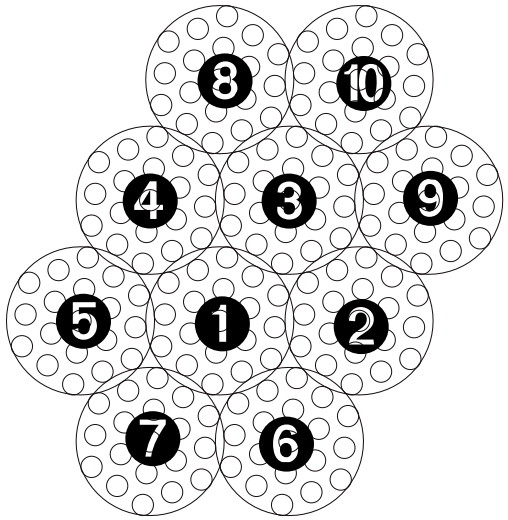


FIG. 2: Schematic representation of the failure event hypothesised to be the weakest-link event by the tight cluster growth model. The composite cross-section is viewed as a patch-work of bundles. In this figure, each bundle is comprised of 19 fibres, obeying equal-load sharing. The failure of a bundle, labelled ❶, causes an overload in its six neighbours. Under this overload, one of them, say ❷ fails. The overloads due to a pair of failed bundles leads to the failure of, say ❸, and so on.

The second model of interest is called the tight cluster growth model [9, 22, 30]. The development of the weakest-link event, according to this model, is depicted schematically in Fig. 2. Here, neighbouring ELS bundles, each comprised of $M$ fibres, hereafter termed $M$-bundles, fail sequentially. The sequence begins with the failure of one $M$-bundle, labelled ❶ in the schematic Fig. 2. The failure of this $M$-bundle overloads its six neighbouring ELS bundles. The second step involves the failure of one of these overloaded ELS $M$-bundles, say ❷, due to the overload. The third step involves the failure of one of the overloaded neighbours of the pair of $M$-bundles ❶, and ❷, and so on. Growth of the cluster of bundles in this manner has been termed 'tight cluster growth' [6].

Let $N_j^{(M,N)}$ denote the number of overloaded neighbouring $M$-bundles surrounding a tight cluster of $j$ $M$-bundles, in a composite comprised of $N$ fibres. Let $N_0^{(M)} \equiv 1$. Let $K_j^{(M,N)}$ denote the stress concentration imposed by this tight cluster on its neighbours. Let $K_0 \equiv 1$. Then, assuming the successive steps of tight cluster growth are approximately independent, the probability of tight cluster growth, $W^{(M,N)}(\sigma;\gamma,\rho)$, can be written as:

$$W^{(M,N)}(\sigma;\gamma,\rho) = \prod_{j=0}^{\lfloor N/M \rfloor - 1} \left\{ 1 - \left[ 1 - E^{(M)}\left( K_j^{(M,N)} \sigma \right) \right]^{N_j^{(M,N)}} \right\}. \tag{14}$$

$W^{(M,N)}(\sigma;\gamma,\rho)$ depends on $\gamma$ through the stress concentrations $K_j^{(M,N)}$, and on $\rho$ through $E^{(M)}(\cdot)$. The upper limit on the index $j$, $\lfloor N/M \rfloor - 1$ indicates the number of $M$ bundles that can fit into the simulation cell of size $N$. The tight cluster growth model thus directly accounts for the finiteness of the system.

Although $K_j^{(M,N)}$, and $N_j^{(M,N)}$ can be evaluated directly following Gupta *et al.* [21], an approximation is presently used to speed up the evaluation of Eq. (14). Consider a tight cluster of $j$ fibre breaks in a simulation cell comprised of $N/M$ fibres. The problems of $j$ $M$-bundles, and $j$ single breaks, differ only in terms of size scale. Also, $K_j^{(M)}$ and $N_j^{(M)}$ are non-dimensional quantities. Therefore, it is presently assumed that

$$K_j^{(M,N)} = K_j^{(1,N/M)}, \quad \text{and} \quad N_j^{(M)} = N_j^{(1,N/M)}. \tag{15}$$

Now, $N/M$ in Eq. (15) need not, in general, be a square number, and may therefore not fit in a rhombus-shaped patch, Fig. 1. Also, it is computationally advantageous if the system size were an even power of two [21]. The approximation

$$K_j^{(M,N)} \approx K_j^{(1,N_1)}, \quad \text{and} \quad N_j^{(M,N)} \approx N_j^{(1,N_1)}, \tag{16}$$

with $N_1 = 2^{2[\log_2 \sqrt{N/M}]}$, addresses these issues. Here, $[\cdot]$ denotes rounding off to the nearest natural number.

$K_j^{(1,N_1)}$ can be directly evaluated following Gupta *et al.* [21]. To evaluate $N_j^{(1,N_1)}$, the tight cluster of $j$-breaks is associated with radius $R$, given by

$$j = \pi R^2. \tag{17}$$

The intact neighbours of a tight cluster of radius $R$ are taken to be those fibres that are broken in a tight cluster of radius $R+1$, but not in one of radius $R$. The number of

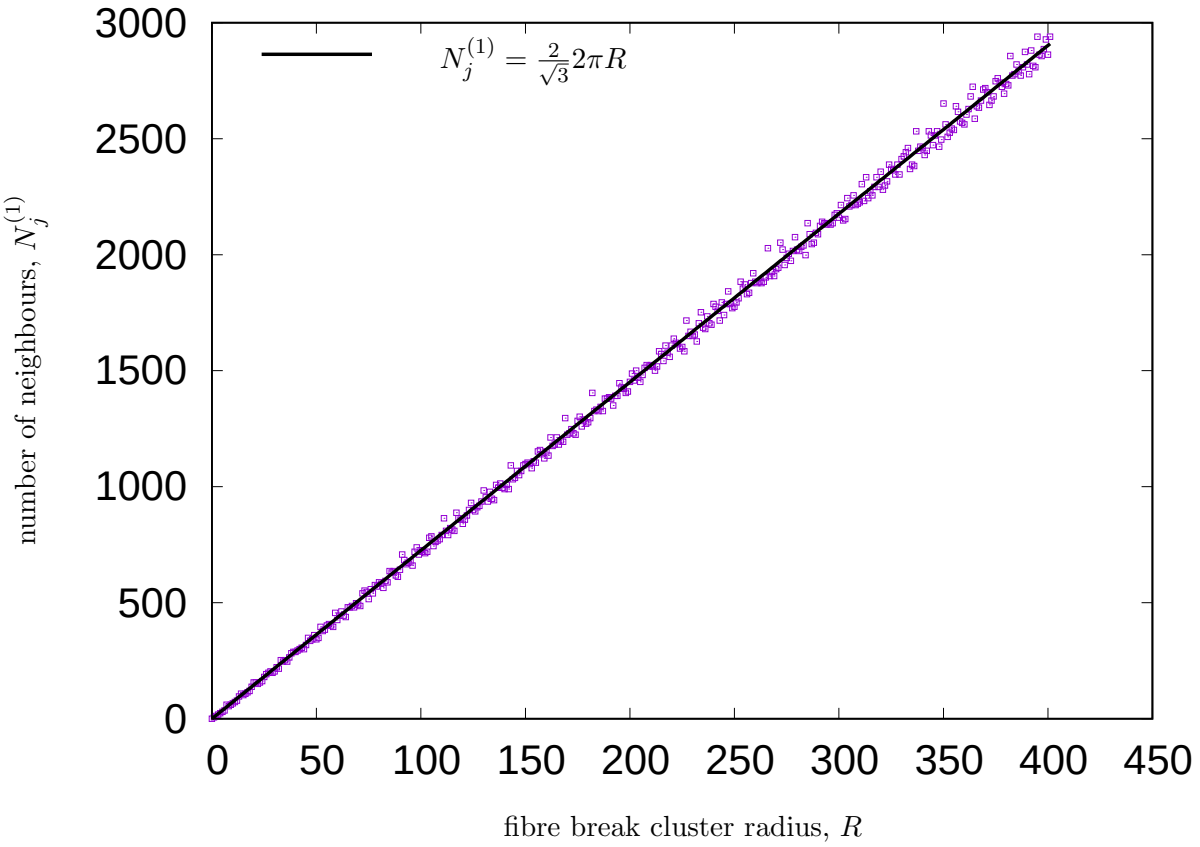


FIG. 3: The number of intact neighbours of penny-shaped clusters of fibre breaks obeys Eq. (18). The system size, $N_1 = 2^{20}$, is much larger than the size of the largest cluster considered.

neighbours can be determined by a simple geometric calculation, and is plotted in Fig. 3. It is seen that

$$N_j^{(1)} = \frac{2}{\sqrt{3}} \times 2\pi R = 4\sqrt{\frac{\pi j}{3}}, \tag{18}$$

captures the empirical scaling very well, provided $j \ll N_1$. However, if $j \approx N_1$, the number of neighbours will be limited by the system size, and is better approximated as $N_j^{(1)} = N_1 - j$. Both possibilities are approximately accounted for by taking

$$N_j^{(1,N_1)} = \min\left(4\sqrt{\pi j/3}, N_1 - j\right). \tag{19}$$

This concludes the discussion of the parameters appearing in Eq. (14).

Let the composite cross-section be *a priori* partitioned into $N/M$ $M$-bundles. Assuming the weakest-link event may initiate from any of these bundles with equal likelihood implies

that

$$G_N(\sigma;\gamma,\rho) = 1 - (1 - W^{(M,N)}(\sigma;\gamma,\rho))^{N/M}. \tag{20}$$

Comparing Eq. (11), and (14) shows that

$$W_N(\sigma;\gamma,\rho) = 1 - (1 - W^{(M,N)}(\sigma;\gamma,\rho))^{1/M}. \tag{21}$$

The case $M = N$ represents a degenerate condition, wherein a single $M$-bundle occupies the entire composite cross-section. In this case, Eqs. (14), and (20) reduce to $G_N(\sigma) = E_M(\sigma)$, where $E_M(\sigma)$ is given either by Eq. (7), or by (10). The tight cluster growth model reduces to the Curtin [20] model if only the first factor were retained in the product of Eq. (14). It reduces to the tight cluster growth model of Mahesh *et al.* [6] by setting $M \equiv 1$.

The tight cluster growth model is more complex than the Curtin [20] model. First, it requires the direct calculation of $K_j^{(M,N)}$, as described above. The Curtin [20] model does not require any stress concentration calculations. Second, the tight cluster growth model requires the evaluation of a product in Eq. (14). This may be computationally intensive, particularly if the individual factors must be evaluated using the McCartney and Smith [28] recursion, Eq. (10).

In return for the added complexity, the tight cluster growth requires only that a single parameter, $M$, be fit. $M$ may be regarded as the counterpart of the fitting parameter $N_c$ in the Curtin [20] model. There is no analog of the Curtin [20] model fitting parameter, $\mu'_{N_c}$, in the tight cluster growth model.

## III. RESULTS, AND DISCUSSION

Monte Carlo fracture simulations have been run on $N_{\text{sim}} = 256$ computer specimen with system sizes, $N \in \{2^{14}, 2^{16}, 2^{18}, 2^{20}\}$, for each Weibull exponent $\rho \in \{1, 2, 3, 5, 10\}$, and for each load-sharing power law exponent $\gamma \in \{0, 1, 1.5, 2, 2.05, 2.1, 2.2, 2.5, 3\}$. Of these $\gamma$, only those in the range $2 < \gamma \leq 3$ represent physical load sharing rules in elastic composites, as noted in Eq. (4). Therefore, attention is focused on this range. This range is of interest also because Hidalgo *et al.* [7] and Roy *et al.* [10] observed a transition within it.

Cluster moments $M_k$, defined in Eq. (6) have been recorded at the point of catastrophic crack propagation from each of these simulations. Specimen strengths are also recorded, and the empirical strength distributions, $G_N(\sigma_{(i)};\gamma,\rho)$, are derived using Eq. (5).

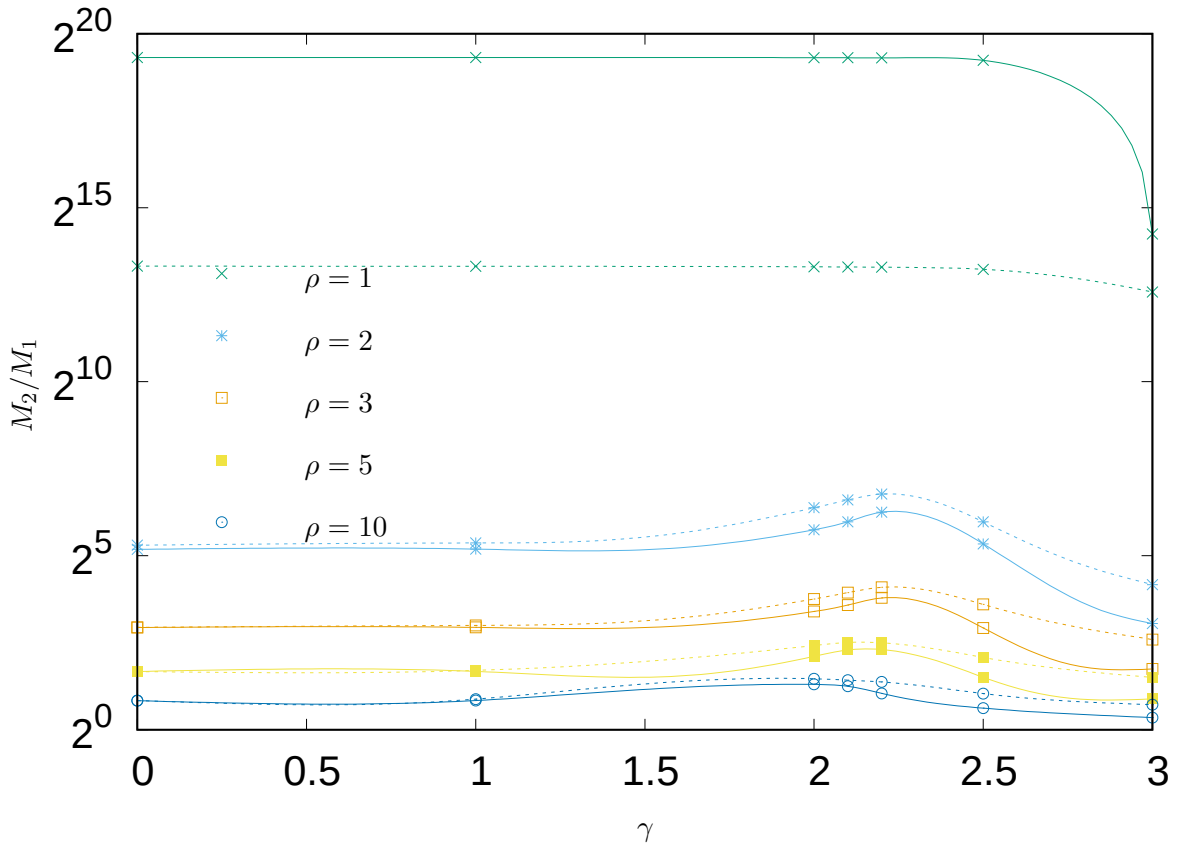


FIG. 4: Variation of the moment ratio, $M_2/M_1$, averaged over all the simulations. Solid lines correspond to system size, $N = 2^{20}$, and dashed lines to $N = 2^{14}$.

### III.1. Cluster statistics

As noted in Sec. II.1.2, Hidalgo *et al.* [7], Pradhan *et al.* [8], Kun *et al.* [25], and Roy *et al.* [10], have used cluster analysis to quantitatively identify the parametric value corresponding to the tough-brittle transition in systems wherein fibre breaks are assumed to be non-interacting. Of these studies, Hidalgo *et al.* [7], and Roy *et al.* [10, Fig. 7], have considered power-law load sharing. The former work assumes Weibull-distributed strengths, with $\rho = 2$, while the latter assume uniform or power-law distributed fibre strengths. They locate the transition at $\gamma = 2.17$, and $\gamma = 2.15$, respectively. The proximity of the transition point despite quite different fibre strength distributions suggests its robustness.

Fig. 4 shows the variation of the moment ratio, $M_2/M_1$ with $\gamma$, for all the presently studied $\rho$, and for two simulation cell sizes, $N = 2^{14}$, and $N = 2^{20}$. For $2 \leq \rho \leq 10$, $M_2/M_1$ maximises at $\gamma \gtrsim 2$, with the maximum moving from $\gamma = 2$ for $\rho = 10$ to $\gamma = 2.2$ for $\rho = 2$.

When $\rho = 1$, $M_2/M_1$ increases from $\gamma = 3$ to $\gamma = 2.5$, and remains nearly constant over $0 \leq \gamma \leq 2.5$. That is, the largest $\gamma$ at which $M_2/M_1$ maximises increases with decreasing $\rho$. These observations hold for both simulation cell sizes.

Applying the criterion of Hidalgo *et al.* [7], and Roy *et al.* [10] to the present results, it is found that the tough-brittle transition occurs at $\gamma = 2$ for $\rho = 10$, and monotonically increases to $\gamma = 2.5$ for $\rho = 1$. The $\gamma$ at which the presently obtained $M_2/M_1$ maximise are comparable to those of Hidalgo *et al.* [7], and Roy *et al.* [10]. It is speculated that for still smaller $\rho < 1$, the transitional $\gamma$ will increase further toward $\gamma = 3$. However, the present results do not clearly indicate if the transitional $\gamma$ will decrease with increasing system size, $N$, for fixed $\rho$. This is because the same transitional $\gamma$ is presently obtained for both the largest and smallest system sizes studied, for all $\rho$. Much larger simulations than those presently feasible will be required to resolve this question.

### III.2. Strength distributions

Fig. 5 shows the empirical strength distributions for $\gamma \in \{3, 2.5, 2\}$ composites with $\rho \in \{10, 1\}$, in Gaussian probability coordinates. These are compared with the best fit lines obtained from the Curtin [20] model. It is seen that in every case, the Curtin [20] model fits the empirical distributions very well. Model parameters $N_c$, and $\mu'_{N_c}$ are fit following the procedure given in Sec. II.2.2. However, only the parameter $N_c$, which is important to understand the tough-brittle transition, is listed in the legends.

Fig. 5a corresponds to the most localised load sharing, with the least fibre strength variability, amongst the cases shown in Fig. 5. In this case, the Curtin [20] model fits the empirical strength distributions of variously sized simulation cells within a relatively narrow range $64 \leq N_c \leq 96$. As the load sharing becomes less localised, with decreasing $\gamma$, the strength distributions approach the corresponding ELS distributions. Thus, for $\gamma = 3$, good fits are obtained using $N_c \ll N$, for both $\rho$ considered. For $\gamma \approx 2$, good fits are obtained only with $N_c \lesssim N$.

In Fig. 6, the same empirical distributions as those in Fig. 5 are fit to the tight cluster growth model, in Weibull probability coordinates. Again, it is seen that in all the cases, good fits are obtained with the tight cluster growth model. The parameter, $M$, is fit for each $\gamma$, and $\rho$; its value is listed in the legends.

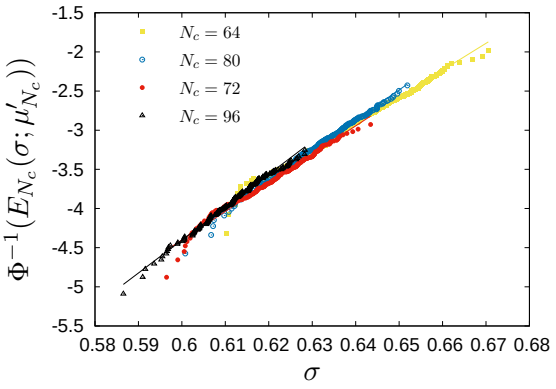


(a) $\gamma = 3$, $\rho = 10$

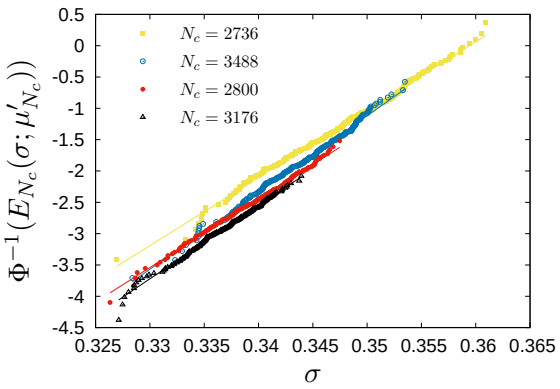


(b) $\gamma = 3$, $\rho = 1$

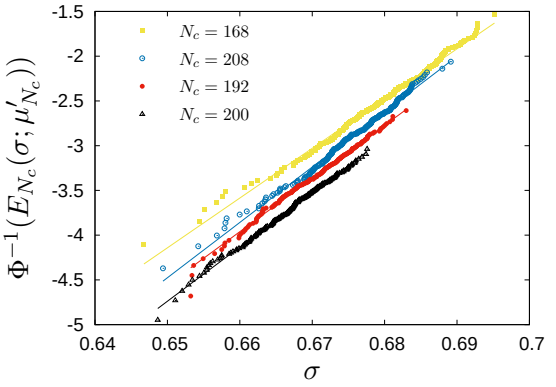


(c) $\gamma = 2.5$, $\rho = 10$

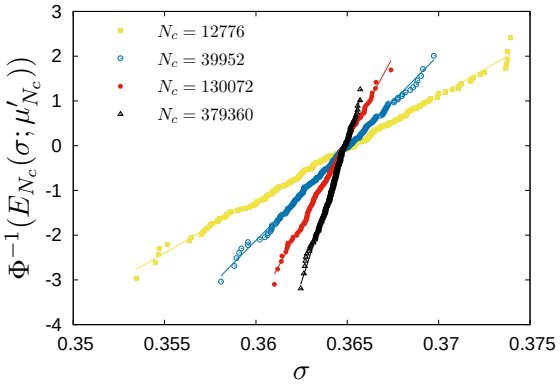


(d) $\gamma = 2.5$, $\rho = 1$

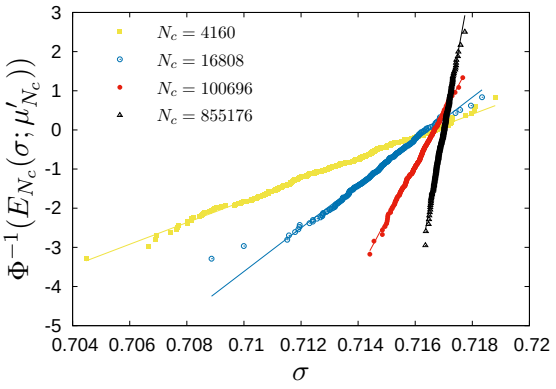


(e) $\gamma = 2$, $\rho = 10$

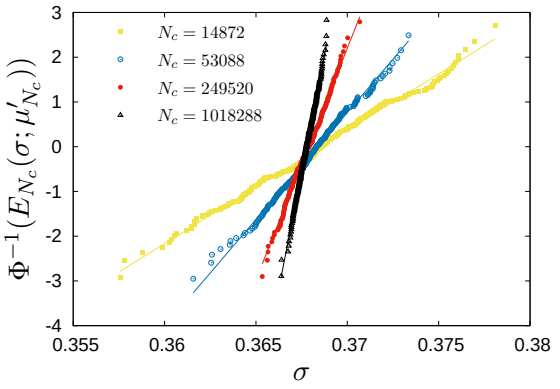


(f) $\gamma = 2$, $\rho = 1$

FIG. 5: Empirical strength distributions of $\gamma \in \{3, 2, 1\}$, $\rho \in \{10, 1\}$ load sharing bundles plotted on Gaussian probability coordinates, and fit with the Curtin [20] model. Each plot shows the empirical strength distribution of $N \in \{2^{14}, 2^{16}, 2^{18}, 2^{20}\}$ composites with yellow, blue, red, and black dots. The model fitting parameter $N_c$ is listed in the legends.

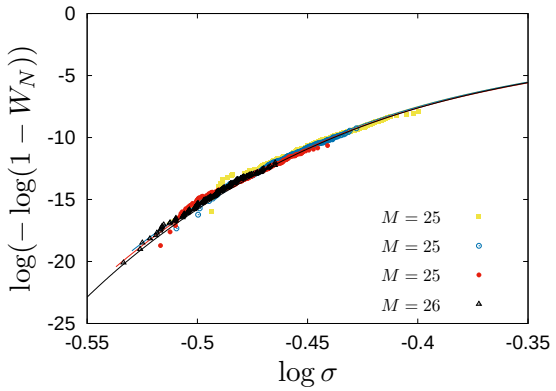


(a) $\gamma = 3$, $\rho = 10$

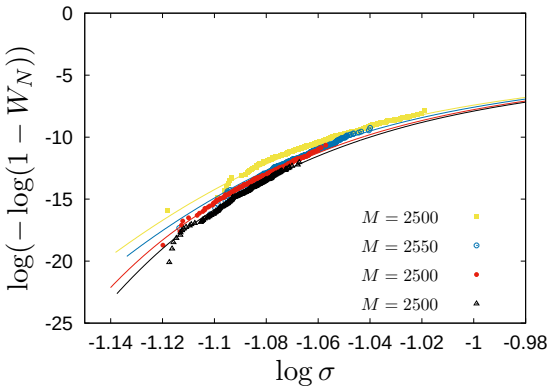


(b) $\gamma = 3$, $\rho = 1$

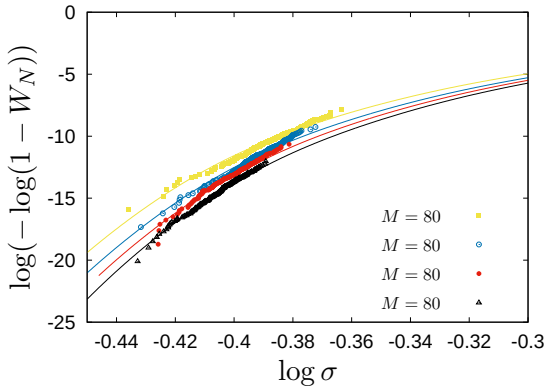


(c) $\gamma = 2.5$, $\rho = 10$

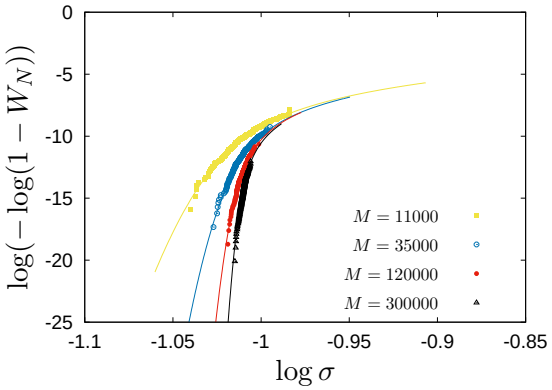


(d) $\gamma = 2.5$, $\rho = 1$

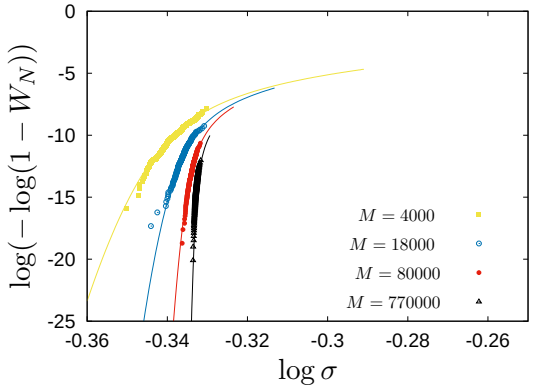


(e) $\gamma = 2$, $\rho = 10$

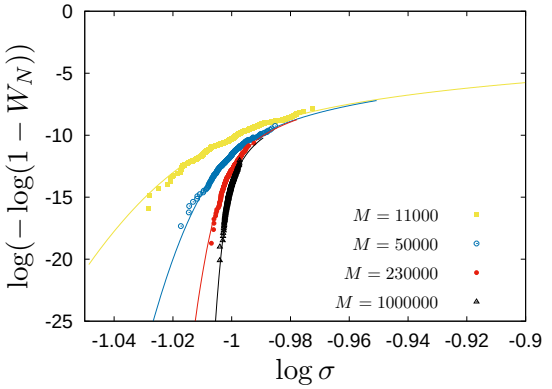


(f) $\gamma = 2$, $\rho = 1$

FIG. 6: Empirical strength distributions of $\gamma \in \{3, 2.5, 2\}$, $\rho \in \{10, 1\}$ load sharing bundles plotted on Weibull probability coordinates, and fit with the tight cluster growth model. Each plot shows the empirical strength distribution of $N \in \{2^{14}, 2^{16}, 2^{18}, 2^{20}\}$ composites, with yellow, blue, red, and black dots, respectively. The model fitting parameter $M$ is listed in the legends.

The weakest-link strength distributions corresponding to different $N$ collapse onto a single master curve only in Fig. 6a, for $\gamma = 3$, $\rho = 10$, with $M = 25$. For all the other cases shown, the classical collapse of the weakest-link distributions into a common master curve [6, 14] is not observed.

Both the Curtin [20] and tight cluster growth models are thus able to fit the empirical strength distributions very well. This is true not only in the probability range of interest, but also in lower the tail of the distribution (not shown). It is known that the predictions of the two models agree for Hedgepeth load sharing, which corresponds to $\gamma = 3$ [30]. The present result extends this conclusion to less localised load sharing rules, viz, $\gamma \leq 3$, also.

The parameter $M$ of the tight cluster growth model is always smaller than $N_c$ of the Curtin [20] model. This is to be expected since $M$ is the size of the initiating cluster leading up to fracture, while $N_c$ is the size of the propagating cluster. However, $M$ is significantly smaller than $N$ only in Figs. 5a–c, and 6a–c. In Figs. 5d–f, and 6d–f, $M \approx N_c$. In the latter cases, the weakest-link product of Eq. (14) in the tight cluster growth model also converges after just one factor, $j = 1$. These observations suggest that with decreasing $\gamma$ and $\rho$, fracture development in the tight cluster growth model approaches that of the Curtin [20] model.

### III.3. Tough-brittle transition

$N_c/N$ in the Curtin [20] model represents the fraction of fibres from which brittle fracture develops. Fig. 7 shows the variation of $N_c/N$ with system size, $N$ on log-log scale for $\rho = 10$, and $\rho = 1$. The points denote the values of $N_c/N$. Lines obtained by least squares fitting are also shown. $N_c/N$ shows a decreasing trend for $2.1 \leq \gamma \leq 3$ in Fig. 7a, which corresponds to $\rho = 10$, implying that the size of cluster of fibre breaks from which brittle fracture initiates scales slower than the system size. This suggests that brittle fracture, i.e., catastrophic crack growth from a localised $N_c$-fibre break nucleus will occur for $2.1 \leq \gamma \leq 3$, as the system size, $N \uparrow \infty$. For $\gamma = 2.05$, neither a clear decreasing nor a clear increasing trend is seen. It is therefore, not possible to decide if the $\beta = 2.05$, $\rho = 10$ specimen will fail by the tough or brittle mode. For $\gamma = 2$, however, $N_c/N$ shows an increasing trend with $N$, implying that the size of the cluster of fibre breaks from which brittle fracture initiates grows faster than the system size. This indicates the tough fracture mode, with $N_c/N \uparrow 1$ with increasing

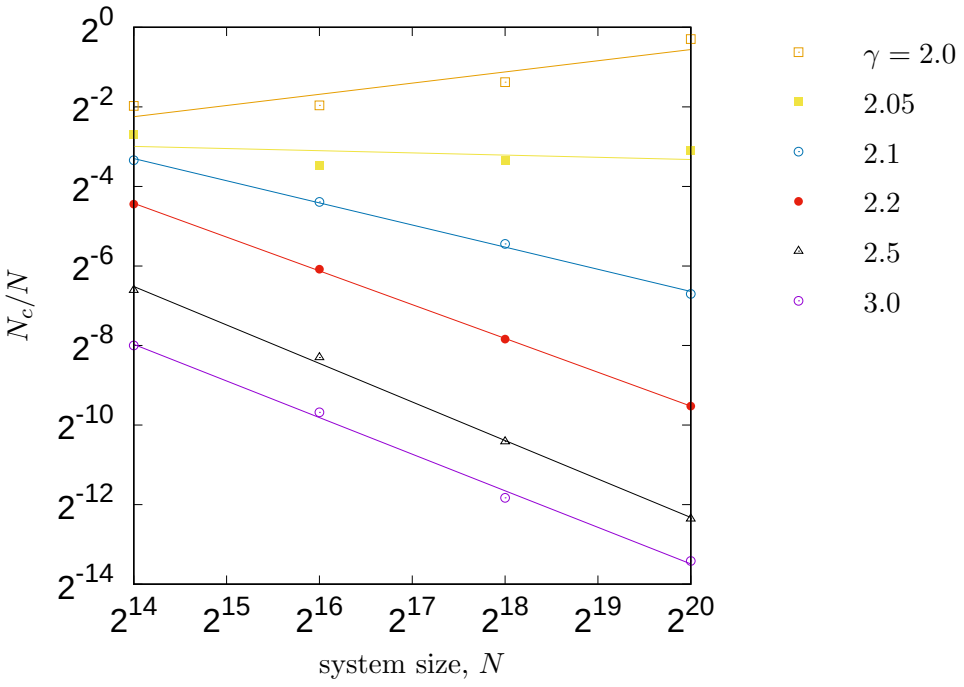


(a) $\rho = 10$

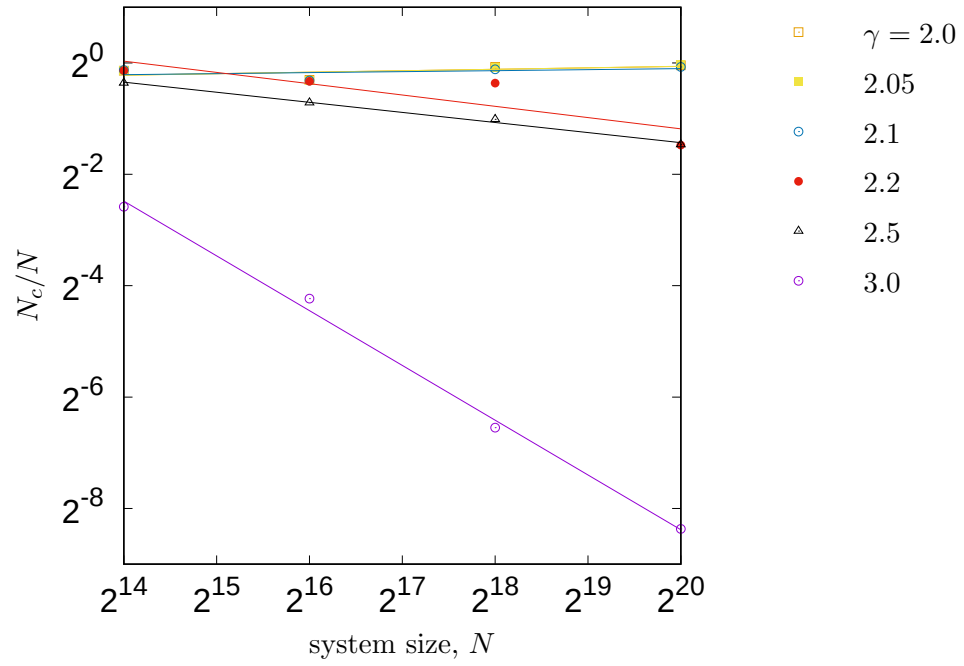


(b) $\rho = 1$

FIG. 7: The scaling of the fraction of the Curtin [20] model bundle size, $N_c/N$, with system size $N$ for various $\gamma$ for (a) $\rho = 10$, and (b) $\rho = 1$ composites.

$N$. The Curtin [20] model thus predicts a tough-brittle transition for $\rho = 10$, for some $\gamma \in [2.0, 2.1]$.

Similar considerations, applied to Fig. 7b, corresponding to $\rho = 1$, reveals a tough-brittle transition at some $\gamma \in [2.1, 2.2]$. Interestingly, this transitional parameter value range includes that ($\gamma \approx 2.17$) obtained by Hidalgo *et al.* [7], and Roy *et al.* [10], assuming no interaction between the fibre breaks, for fibre Weibull exponent $\rho = 2$.

In the tight cluster growth model, $M/N$ denotes the fraction of fibres from which brittle fracture may develop. The variation of $M/N$ with system size, $N$ on log-log scale for $\rho = 10$, and $\rho = 1$ are shown in Fig. 8. Again, the points denote the calculated values of $M/N$, and the lines are obtained by linear least squares fitting the points. For $\rho = 10$, a decreasing trend of $M/N$ with $N$ can be seen in Fig. 8a for $2.05 \leq \gamma \leq 3$, which indicates the brittle failure mode. The $M/N$ corresponding to $\gamma = 2$, however, shows an increasing trend with $N$, which again points to the tough mode. The tough-brittle transition must therefore, occur over the interval $\gamma \in [2, 2.05]$. In Fig. 8b, for $\rho = 1$, the $\gamma = 2.1$ and 2.05 lines are nearly horizontal. The scatter of the data points about their least squares lines is also significant. Therefore, the fracture mode in these cases is ambiguous. For $\gamma = 2$, however, a positive slope, and therefore, the tough mode is clearly indicated.

TABLE I: Ranges of the power-law load sharing exponent, $\gamma^*$, over which the tough-brittle transition is predicted to occur by the three approaches. $\rho$ denotes the Weibull exponent of the fibre strengths.

| | $\rho = 10$ | $\rho = 1$ |
|---|---|---|
| Cluster analysis | $\gamma^* \in [2.0, 2.1]$ | $\gamma^* \in [2.0, 2.5]$ |
| Curtin [20] model | $\gamma^* \in [2.0, 2.1]$ | $\gamma^* \in [2.0, 2.2]$ |
| Tight cluster growth model | $\gamma^* \in [2.00, 2.05]$ | $\gamma^* \in [2.0, 2.2]$ |

Table I summarises the $\gamma^*$ range over which the tough-brittle transition is predicted by cluster analysis, by the Curtin [20] model, and by the tight cluster growth model. Regardless of the method, the $\gamma^*$ range is wider for the smaller Weibull exponent, $\rho = 1$, than for $\rho = 10$. Also, for fixed $\rho$, the latter two methods, based on analysing the strength distribution, provide tighter bounds on the transitional $\gamma^*$. It seems plausible that the $\gamma^*$-ranges can be further narrowed if fracture simulations could be performed on even larger system sizes,

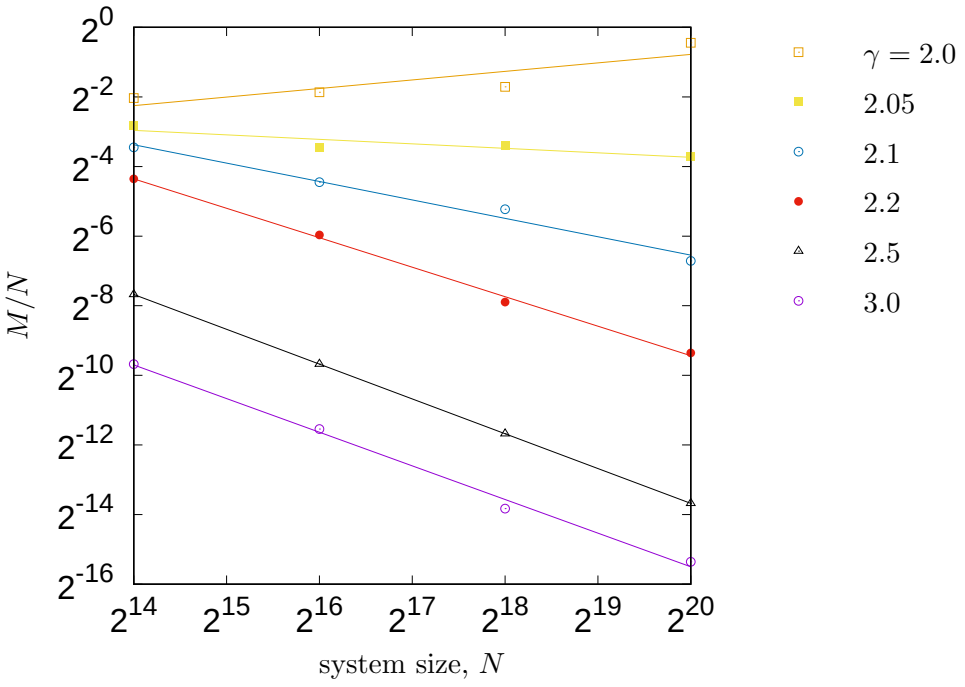


(a) $\rho = 10$

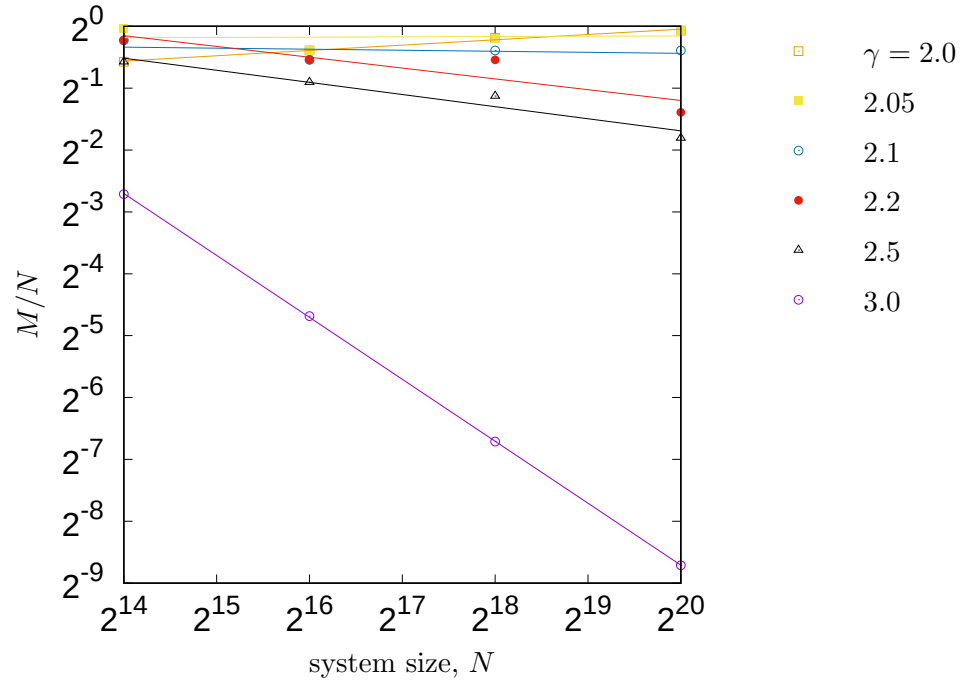


(b) $\rho = 1$

FIG. 8: The scaling of the fraction of the tight cluster growth model bundle size, $M/N$, with system size $N$ for various $\gamma$ for (a) $\rho = 10$, and (b) $\rho = 1$ composites.

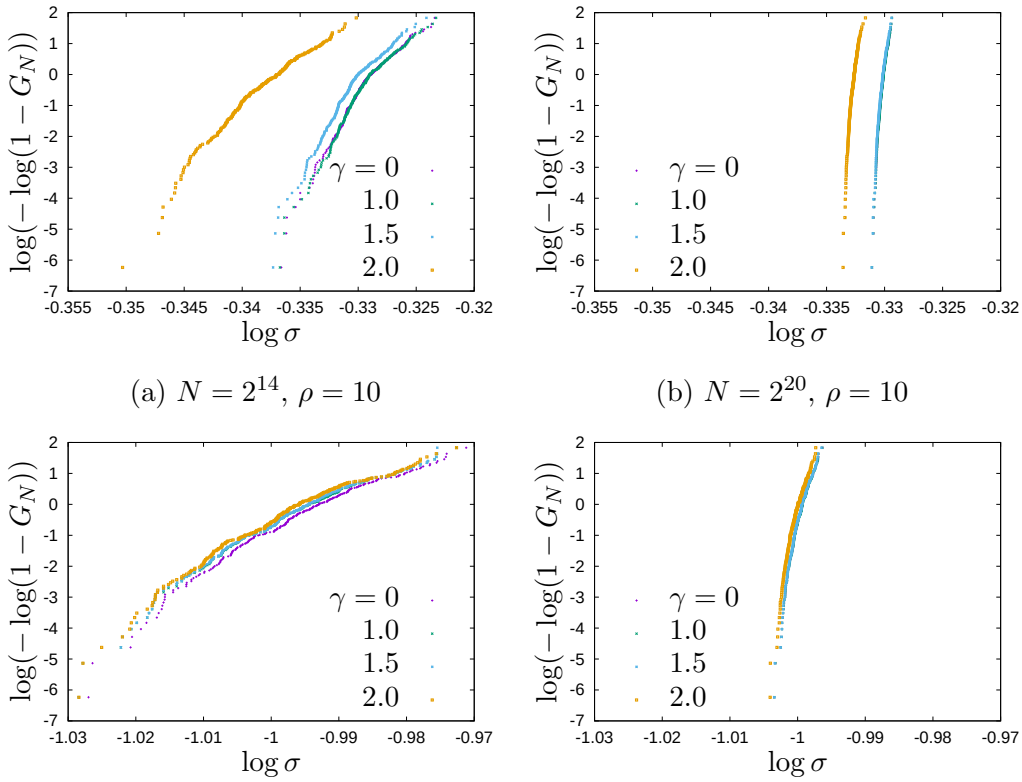


(a) $N = 2^{14}$, $\rho = 10$

(b) $N = 2^{20}$, $\rho = 10$

(c) $N = 2^{14}$, $\rho = 1$

(d) $N = 2^{20}$, $\rho = 1$

FIG. 9: Empirical strength distributions obtained from Monte Carlo simulations with load sharing exponent $\gamma \in \{0, 1, 1.5, 2\}$. The first row corresponds to $\rho = 10$, and the second row to $\rho = 1$. The first and second columns correspond to system sizes $N = 2^{14}$, and $2^{20}$, respectively.

$N > 2^{20}$. It is speculated that for large enough $N$, $\gamma^* \downarrow 2$, for all Weibull exponents $\rho$.

### III.4. The load sharing regime $0 \leq \gamma \leq 2$

It was noted in connection with Eq. (4) that the regime $0 \leq \gamma \leq 2$ cannot be realised in physical elastic composites, because the load redistribution in this regime also depends on system size, $N$. In this regime, the increasing trend of $N_c/N \uparrow 1$ and $M/N \uparrow 1$ with system size $N$, observed for $\gamma = 2$ in Figs. 7, and 8 can be expected to hold. Thus, for sufficiently large $N$, the strength distributions of these composites will be given by Eq. (7), derived for ELS bundles [13].

The convergence of the $0 < \gamma \leq 2$ empirical strength distributions toward the $\gamma = 0$ ELS

distribution can be directly demonstrated. Fig. 9 shows these distributions for $N \in \{2^{14}, 2^{20}\}$ composites with $\gamma \in \{0, 1, 1.5, 2\}$. The first row corresponds to $\rho = 10$, and the second row to $\rho = 1$. The first column corresponds to the small system size $N = 2^{14}$, while the second corresponds to the larger size $N = 2^{20}$. The variability of the composite strengths in the second column is clearly much smaller than that in the first column. Empirical distributions corresponding to all the four $\gamma$ are seen distinctly in the first column. In the second column, corresponding to the larger system size, the empirical distributions corresponding to $\gamma = 0$, 1, and 1.5 are observed to overlap. The distribution corresponding to $\gamma = 2$ is also to seen to approach that for $\gamma = 0$ with increasing $N$, but not to overlap.

## IV. CONCLUSION

The influence of load sharing on the fracture mode of unidirectional composites in a transverse plane by fibre breakage has been studied through Monte Carlo fracture simulations over a range of load sharing exponent, $\gamma$, and fibre strength variability. Interactions, which ensure traction-free fibre breaks, are accounted for in the fracture simulations. The pattern of fibre breaks just before catastrophic crack propagation begins has been interpreted using cluster analysis. The empirical strength distributions given by the simulations have been interpreted using two stochastic models of composite failure, viz., the Curtin [20] model, and the tight cluster growth model [9, 22, 30]. All the approaches point to a tough-brittle transition near $\gamma = 2$. On the one hand, for $\gamma \gtrsim 2$, brittle fracture ensues from a critical cluster of fibre breaks, which becomes increasingly localised with increasing system size. On the other hand, for $\gamma \lesssim 2$, the size of the critical cluster grows faster than the system size, which will result in the tough fracture mode for sufficiently large systems.

---


[1] B. Majumdar, T. Matikas, and D. Miracle, Experiments and analysis of fiber fragmentation in single and multiple-fiber SiC/Ti-6Al-4V metal matrix composites, Composites Part B: Engineering **29**, 131 (1998).

[2] W. Curtin, Dimensionality and size effects on the strength of fiber-reinforced composites, Composites Science and Technology **60**, 543 (2000).

[3] D. Gücer and J. Gurland, Comparison of the statistics of two fracture modes, J Mech Phys Solids **10**, 365 (1962).

[4] R. Smith, S. Phoenix, M. Greenfield, R. Henstenburg, and R. Pitt, Lower-tail approximations for the probability of failure of three-dimensional fibrous composites with hexagonal geometry, Proc. R. Soc. Lond. A **388**, 353 (1983).

[5] I. Beyerlein, S. Phoenix, and A. Sastry, Comparison of shear-lag theory and continuum fracture mechanics for modeling fiber and matrix stresses in an elastic cracked composite lamina, Int J Solids Str **33**, 2543 (1996).

[6] S. Mahesh, S. Phoenix, and I. Beyerlein, Strength distributions and size effects for 2D and 3D composites with Weibull fibers in an elastic matrix, Int J Fracture **115**, 41 (2002).

[7] R. C. Hidalgo, Y. Moreno, F. Kun, and H. J. Herrmann, Fracture model with variable range of interaction, Physical review E **65**, 046148 (2002).

[8] S. Pradhan, B. K. Chakrabarti, and A. Hansen, Crossover behavior in a mixed-mode fiber bundle model, Phys. Rev. E **71**, 036149 (2005).

[9] C. N. I. Habeeb and S. Mahesh, Strength distribution of planar local load-sharing bundles, Physical Review E **92**, 022125 (2015).

[10] S. Roy, S. Biswas, and P. Ray, Modes of failure in disordered solids, Physical Review E **96**, 063003 (2017).

[11] W. Weibull, A statistical distribution function of wide applicability, Journal of applied mechanics **103**, 293 (1951).

[12] S. Biswas, S. Roy, and P. Ray, Nucleation versus percolation: Scaling criterion for failure in disordered solids, Physical Review E **91**, 050105(R) (2015).

[13] H. Daniels, The statistical theory of the strength of bundles of threads. I, Proc. R. Soc. Lond A **183**, 405 (1945).

[14] D. F. Harlow and S. L. Phoenix, The chain-of-bundles probability model for the strength of fibrous materials I, J. compos. mater. **12**, 195 (1978).

[15] S. Mahesh and S. L. Phoenix, Absence of a tough-brittle transition in the statistical fracture of unidirectional composite tapes under local load sharing, Phys. Rev. E **69**, 026102 (2004).

[16] J. M. Hedgepeth, *Stress concentrations in filamentary structures*, Tech. Rep. TN D 882 (NASA, 1961).

[17] J. M. Hedgepeth and P. Van Dyke, Local stress concentrations in imperfect filamentary composite materials, J. Compos. Mater. **1**, 294 (1967).

[18] H. Suemasu, An analytical study of probabilistic aspects of strength of unidirectional fiber reinforced composites under tensile loads, Japan Society for Composite Materials, Transactions **8**, 29 (1982).

[19] S. Zhou and W. Curtin, Failure of fiber composites: a lattice Green function model, Acta Metallurgica et Materialia **43**, 3093 (1995).

[20] W. A. Curtin, Size scaling of strength in heterogeneous materials, Phys Rev Lett **80**, 1445 (1998).

[21] A. Gupta, S. Mahesh, and S. M. Keralavarma, A fast algorithm for the elastic fields due to interacting fibre breaks in a periodic fibre composite, International Journal of Fracture **211**, 295 (2018).

[22] S. Mahesh, A. Gupta, U. S. Kachhwah, and N. Sheikh, A fast algorithm to simulate the failure of a periodic elastic fibre composite, International Journal of Fracture **217**, 127 (2019).

[23] M. Rezghi and L. Eldén, Diagonalization of tensors with circulant structure, Linear Algebra and its Applications **435**, 422 (2011).

[24] S. Mahesh, I. J. Beyerlein, and S. L. Phoenix, Size and heterogeneity effects on the strength of fibrous composites, Physica D: Nonlinear Phenomena **133**, 371 (1999).

[25] F. Kun, S. Zapperi, and H. J. Herrmann, Damage in fiber bundle models, The European Physical Journal B-Condensed Matter and Complex Systems **17**, 269 (2000).

[26] J. Hoshen and R. Kopelman, Percolation and cluster distribution. i. cluster multiple labeling technique and critical concentration algorithm, Physical Review B **14**, 3438 (1976).

[27] T. Cormen, C. Leiserson, R. Rivest, and C. Stein, *Introduction To Algorithms* (MIT Press, 2001).

[28] L. McCartney and R. Smith, Statistical theory of the strength of fiber bundles, Journal of applied mechanics **50**, 601 (1983).

[29] A. Hansen, P. C. Hemmer, and S. Pradhan, *The fiber bundle model: modeling failure in materials* (John Wiley & Sons, 2015).

[30] A. Gupta, S. Mahesh, and S. M. Keralavarma, Strength distribution of large unidirectional composite patches with realistic load sharing, Physical Review E **96**, 043002 (2017).